

REPORTS

- cycles with 10 pools per cycle [K. Burgess, A. I. Liaw, and N. Wang. *J. Med. Chem.* **37**, 2985 (1994)].
31. An impurity in the LCMS chromatogram, which was ^1H NMR-silent and had an isotope pattern in its mass spectrum consistent with an osmium-containing substance, was not included in calculating the purity of product **8**.
32. We gratefully acknowledge M. Narovlyansky for providing macrobeads **1**; Q. Liao, P. Wang, and J. Dudek for HRMS

analysis; J. Raggio, L. Castro, and J. Tallarico for providing encoding reagents and for cleaving and analyzing chemical tags; Y.-K. Kim for helpful discussions regarding the transformation of **3** \rightarrow **4**; and M. Kanan for thoughtful review of this manuscript. Supported by the NIGMS and the NCI.S.L.S. is an Investigator at the Howard Hughes Medical Institute at Harvard. M.D.B. is an HHMI predoctoral fellow, and E.M.B. is an HHMI undergraduate fellow.

Supporting Online Material

www.sciencemag.org/cgi/content/full/302/5645/613/DC1
Materials and Methods
Tables S1 to S7

31 July 2003; accepted 22 September 2003

Experimental Models of Primitive Cellular Compartments: Encapsulation, Growth, and Division

Martin M. Hanczyc,* Shelly M. Fujikawa,* Jack W. Szostak†

The clay montmorillonite is known to catalyze the polymerization of RNA from activated ribonucleotides. Here we report that montmorillonite accelerates the spontaneous conversion of fatty acid micelles into vesicles. Clay particles often become encapsulated in these vesicles, thus providing a pathway for the prebiotic encapsulation of catalytically active surfaces within membrane vesicles. In addition, RNA adsorbed to clay can be encapsulated within vesicles. Once formed, such vesicles can grow by incorporating fatty acid supplied as micelles and can divide without dilution of their contents by extrusion through small pores. These processes mediate vesicle replication through cycles of growth and division. The formation, growth, and division of the earliest cells may have occurred in response to similar interactions with mineral particles and inputs of material and energy.

The bilayer membranes that surround all present-day cells and act as boundaries are thought to have originated in the spontaneous self-assembly of amphiphilic molecules into membrane vesicles (1–5). Simple amphiphilic molecules have been found in meteorites (6–7) and have been generated under a wide variety of conditions in the laboratory, ranging from simulated ultraviolet irradiation of interstellar ice particles (8) to hydrothermal processing under simulated early Earth conditions (9, 10). Molecules such as simple fatty acids can form membranes when the pH is close to the pK_a (K_a is the acid dissociation equilibrium constant) of the fatty acid carboxylate group in the membrane (3, 11). Hydrogen bonding between protonated and ionized carboxylates may confer some of the properties of more complex lipids with two acyl chains, thus allowing the formation of a stable bilayer phase (11, 12). Fatty acid vesicles may be further stabilized (to a wider range of pH and even to the presence of other simple amphiphiles such as fatty alcohols and fatty acid glycerol esters. Recent studies have shown that saturated fatty acid/

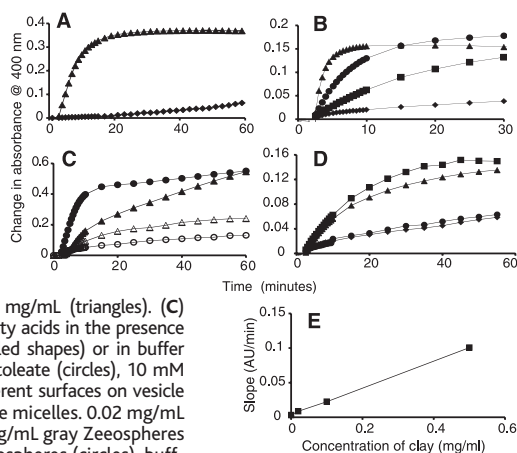
fatty alcohol mixtures with carbon chain lengths as short as 9 can form vesicles capable of retaining ionic fluorescent dyes, DNA, and proteins (4).

Vesicles consisting of simple amphiphilic molecules could have existed under plausible prebiotic conditions on the early Earth, where they may have produced distinct chemical microenvironments that could retain and protect primitive oligonucleotides while potentially allowing small molecules such as activated mononucleotides to diffuse in and out

of the vesicle. Furthermore, compartmentalization of replicating nucleic acids (or some other form of localization) is required to enable Darwinian evolution by preventing the random mixing of genetic polymers, thus coupling genotype and phenotype (13). If primordial nucleic acids assembled on mineral surfaces (14–17), the question arises as to how they eventually came to reside within membrane vesicles. Although dissociation from the mineral surface followed by encapsulation within newly forming vesicles (perhaps in a different location under different environmental conditions) is certainly a possibility, a direct route would be more satisfying and perhaps more efficient. The unexpected interaction between mineral surfaces and membrane-forming amphiphiles described here could provide such a pathway.

In the course of exploring the autocatalytic assembly of myristoleate (C14) vesicles from myristoleate micelles (18), we examined the effect of other negatively charged surfaces on vesicle assembly. We found that the addition of small quantities of montmorillonite to the reaction mixture resulted in an increase in the initial rate of the vesicle assembly reaction by a factor of 100 (19) (Fig. 1A). The magnitude of the rate acceleration increased linearly with increasing concentrations of added montmorillonite, as expected from a rate-limiting process occurring on the mineral surface (Fig. 1, B and E). The effect is clearly catalytic, because the membrane

Fig. 1. Turbidity curves showing vesicle formation over time. Fatty acid micelles were added at 2 min to a buffered solution (0.2 M Na^+ -bicine, pH 8.5) with or without suspended particles as indicated. (A) Myristoleate (10 mM) added to buffer with 0.6 mg/mL montmorillonite (triangles) or to buffer only (diamonds). (B) Effect of varying concentrations of montmorillonite on vesicle formation. Buffer only (diamonds), 0.02 mg/mL (squares), 0.1 mg/mL (circles), 0.5 mg/mL (triangles). (C) Vesicle formation from different fatty acids in the presence of montmorillonite (0.5 mg/mL, filled shapes) or in buffer alone (open shapes). 10 mM palmitoleate (circles), 10 mM oleate (triangles). (D) Effect of different surfaces on vesicle formation from 10 mM myristoleate micelles. 0.02 mg/mL montmorillonite (squares), 0.02 mg/mL gray Zeospheres (triangles), 0.02 mg/mL white Zeospheres (circles), buffer alone (diamonds). (E) Initial rate of vesicle formation [from (B)] versus montmorillonite concentration.



Howard Hughes Medical Institute and Department of Molecular Biology, Massachusetts General Hospital, Boston, MA 02114, USA.

*These authors contributed equally to this work.
†To whom correspondence should be addressed. E-mail: szostak@mcbio.mgh.harvard.edu

surface area generated can be greater by a factor of 50 than the maximum possible surface area of the clay calculated as separated sheets. (The actual membrane/clay surface ratio is probably much greater, because clay particles consist of stacked sheets.) Furthermore, the clay particles affect the rate of

vesicle formation, but the critical aggregate concentration was unchanged, showing that the micelle-vesicle equilibrium was not affected (fig. S1). Montmorillonite also increased the rate of vesicle formation for longer-chain unsaturated fatty acids such as palmitoleic (C16) and oleic (C18) acids (Fig. 1C). Because saturated fatty acids are much more likely prebiotic molecules than are unsaturated fatty acids, we examined the micelle-to-vesicle transition of the C14 saturated fatty acid myristic acid and observed a similar rate acceleration in the presence of montmorillonite (fig. S2).

Because both vesicles and montmorillonite clay have negatively charged surfaces (with an associated layer of loosely bound positive counterions), we examined the ability of other surfaces of varying charge densities to accelerate vesicle assembly. Other silicate, aluminosilicate, and borosilicate surfaces strongly accelerate vesicle assembly. A variety of negatively charged cross-linked agarose or dextran beads had little or no effect. Hydroxyapatite particles became coated with fatty acid but did not accelerate vesicle formation. Synthetic negatively charged alumino-silicate ceramic microspheres [gray Zeospheres (3M)] were efficient catalysts of vesicle assembly, although less effective than montmorillonite on a weight basis, probably because of their lower surface/mass ratio. Synthetic ceramic microspheres with a lower surface charge density (white Zeospheres) were less effective (Fig. 1D), further supporting the idea that surface charge density is a critical factor in the acceleration of vesicle assembly.

In clay-mediated reactions, vesicles were visible within 1 min and ranged from <0.5 μm to >30 μm in diameter. The ceramic microspheres were easily distinguished, even in close association with vesicles. The gray Zeospheres were encapsulated within vesicles (Fig. 2, A to D), whereas less effective white Zeospheres were rarely encapsulated. Montmorillonite particles were more heterogeneous and difficult to visualize, but many appeared coated with small vesicles and also were trapped within product vesicles (Fig. 2, E to H). Both gray Zeospheres and clay particles were observed inside composite vesicles consisting of numerous small vesicles inside one or more large vesicles (Fig. 2, B, D, and H). These composite vesicles strongly suggest that many vesicles can form in proximity to a single mineral particle and can become trapped within a large encompassing vesicle.

We hypothesize that a layer of positively charged cations associated with or adjacent to the mineral surface attracts negatively charged micelles or free fatty acid molecules, facilitating their aggregation into a bilayer membrane. This process may be similar to the adsorption and aggregation of charged colloidal particles on a surface of opposite charge (20, 21). Membranes formed in this way could in turn expand by absorbing additional fatty acid, coming to encapsulate the mineral particle along with any additional vesicles subsequently formed at the mineral surface. We suggest that a similar surface-mediated membrane organization may explain at least part of the strong autocatalytic effect of preformed vesicles on the conversion of fatty acid micelles into vesicles.

Enhanced prebiotic encapsulation of mineral particles within membrane vesicles would bring the catalytic potential of the mineral surfaces into the membrane vesicle. For example, oligonucleotides might be synthesized inside vesicles on the surface of encapsulated clay particles. Alternatively, oligonucleotides synthesized on the surface of free clay particles could subsequently become encapsulated within membrane vesicles. To examine this possibility, we prepared montmorillonite clay loaded with a fluorescently labeled RNA oligonucleotide (Cy3-A₁₅) (19). Excess unbound or weakly bound RNA was removed by washing with buffer, after which the clay sample was used in a vesicle assembly reaction. Some of the resulting vesicles contained RNA-loaded clay particles in their interiors (Fig. 2I). To address whether RNA molecules that did dissociate from the clay surface would remain inside the vesicle, we separately prepared vesicles containing encapsulated free Cy3-RNA and removed unencapsulated RNA by size-exclusion chromatography. No leakage of the RNA from the vesicles was observed over a 24-hour period (Fig. 2J).

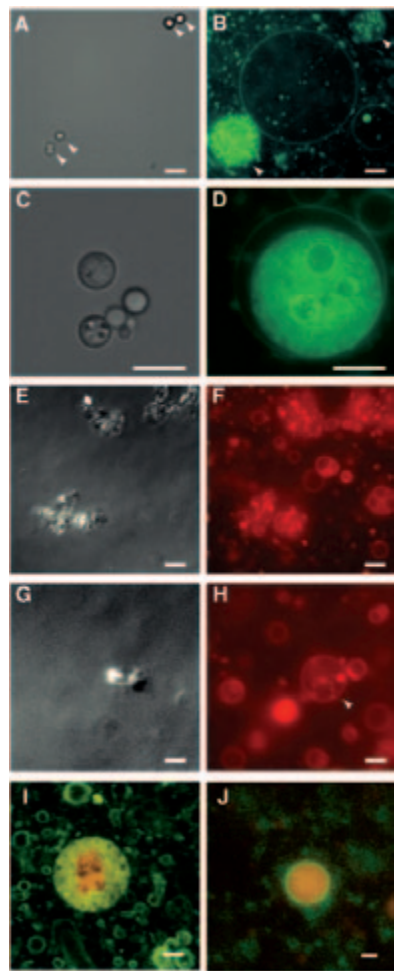


Fig. 2. Light micrographs of particles and vesicles. Particles visualized with Nomarski optics (A, C, E, and G) and dye-labeled vesicles visualized by fluorescence (B, D, F, H, I, and J). (A and B) Gray Zeospheres encapsulated within myristoleate vesicles. Arrowheads indicate Zeospheres in (A) and vesicles containing the Zeospheres in (B). (C and D) Close-up image of gray Zeospheres encapsulated within a vesicle. (E and F) Montmorillonite associated with myristoleate vesicles. (G and H) Montmorillonite encapsulated within myristoleate vesicles (arrowhead indicates vesicle containing clay particles). Size bar for (A) to (H), 5 microns. (I) Montmorillonite coated with Cy3-labeled RNA (red) trapped inside dye-labeled vesicles (green). (J) Cy3-labeled RNA (red) in solution encapsulated within labeled vesicle (green). Size bar for (I) and (J), 1 micron.

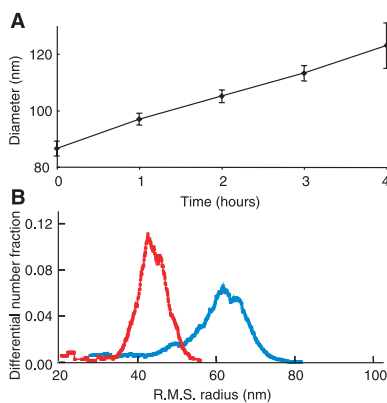


Fig. 3. Growth of myristoleate vesicles in response to feeding with one equivalent of myristoleate micelles over a 4-hour period. Changes in vesicle size were followed by (A) dynamic light scattering (DLS) (three replicates) and (B) physical separation by flow-field fractionation coupled with size analysis by multiangle laser-light scattering (FFF-MALLS). RMS, root mean square.

REPORTS

By catalyzing the assembly of both bilayer membrane vesicles and nucleic acid polymers, and by promoting the union of these two fundamental building blocks of cellular life, mineral particles may have greatly facilitated the emergence of the first cells. Although primordial nucleic acid genomes could in principle replicate through ribozyme-like catalytic activities (13, 22), the first cell membranes must have been able to replicate spontaneously because of the absence of any biomolecular machinery to direct growth and division. Here we describe processes that result in the spontaneous growth and division of fatty acid vesicles. Our vesicle growth experiments are based on earlier work in which a large excess of oleate (C18) micelles at high pH were added to preformed oleate or phospholipid vesicles buffered at lower pH; the preformed vesicles increased in size as a result of the incorporation of the oleate into the bilayer membrane of the vesicles (23, 24). However, a large number of new vesicles were also observed, suggesting that much of the added oleate had formed new vesicles.

We reasoned that vesicle growth could be enhanced and the formation of new vesicles reduced by eliminating the transiently high micelle concentration present immediately after micelle addition to vesicles. We therefore added dilute fatty acid micelles to preformed vesicles slowly, over a 4-hour period. We chose to work with myristoleate vesicles because these vesicles are more permeable to small polar molecules than are oleate (or phospholipid) vesicles, allowing faster osmotic equilibration with the external buffer after membrane growth. To follow vesicle growth quantitatively, we monitored the size of the vesicles over the course of the reaction, using 90° dynamic light scattering (DLS) (19). Examination of an initial population of myristoleate vesicles, prepared by extrusion through 100-nm pore filters (25), revealed an average diameter of approximately 87 ± 3 nm. Slow addition of one equivalent of myristoleate micelles over a period of 4 hours resulted in a steady increase in average vesicle size, up to a final mean diameter of 123 ± 8 nm, consistent with quantitative incorporation of the new myristoleate into the preformed vesicles and leading to a doubling of surface area ($123^2/87^2 \sim 2$) (Fig. 3A). Because DLS analysis cannot distinguish between the growth of preformed vesicles and the formation of new, larger vesicles, we examined the same vesicle populations, using a method that physically separates particles on the basis of size [flow-field fractionation (FFF)], coupled with a different light-scattering approach to size measurement, multi-angle laser light scattering (MALLS) (19, 26). This analysis revealed that the entire population of vesicles had shifted to a larger size by

the end of the growth experiment, with little overlap between initial and final size distributions, showing that almost all vesicles experienced at least some growth (Fig. 3B).

To directly measure the fraction of added fatty acid that became incorporated into the preexisting vesicles, we used a fluorescence resonance energy transfer (FRET) assay based on membrane-localized fluorescent dyes (19, 27, 28). As the vesicles with both donor and acceptor dyes grow by incorporating new fatty acid, the average distance between donor and acceptor molecules increases, resulting in a decrease in FRET efficiency [monitored by measuring the donor/acceptor fluorescence ratio ($F_{\text{don}}/F_{\text{acc}}$), normalized to the $F_{\text{don}}/F_{\text{acc}}$ after detergent lysis]. The dyes we used exchange extremely slowly between phospholipid vesicles (27). The negligible rate of dye exchange between myristoleate vesicles can be seen both visually (fig. S3) and by the absence of any significant change in FRET efficiency after the addition of unlabeled vesicles to doubly labeled vesicles (Fig. 4B, initial versus control vesicles). Therefore, dye dilution in our experiments can only occur through growth of the preformed membrane. A standard curve of the normalized $F_{\text{don}}/F_{\text{acc}}$ versus the fatty acid/dye ratio was generated (Fig. 4A) and used to calibrate experimental measurements of FRET efficiency during vesicle growth experiments. Results from replicate 4-hour growth experiments (Fig. 4B) show that $\sim 90\%$ of the fatty acid in added micelles became incorporated into the preformed vesicles, consistent with our observations of vesicle growth and confirming

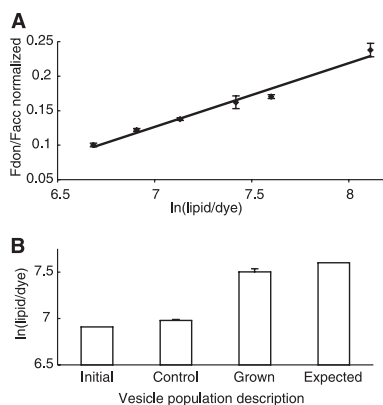


Fig. 4. FRET assay for membrane growth. (A) Standard curve of normalized $F_{\text{don}}/F_{\text{acc}}$ versus $\ln(\text{fatty acid/dye})$ in myristoleate vesicles (three replicates). (B) Analysis of $\ln(\text{fatty acid/dye})$ for the initial vesicle population (before growth), a control population of doubly labeled vesicles 4 hours after the addition of one volume of equimolar unlabeled vesicles (three replicates), grown vesicle population (three replicates), and for comparison the expected ratio assuming 100% fatty acid incorporation into the preexisting vesicle population during growth.

that new vesicle formation is a minor pathway under these conditions. In summary, we have shown by several independent methods that myristoleate vesicles can grow efficiently by incorporating additional fatty acid from slowly added micelles.

To induce vesicle division, we have adapted the process of extrusion through small-pore polycarbonate membrane filters (19, 29, 30). The mechanism by which extrusion leads to vesicle size decrease is not well understood (31–33), but the existing data are consistent with a model in which a vesicle enters the pore under pressure, transforms to a roughly spherocylindrical shape, and fragments into smaller vesicles with a diameter somewhat smaller than the pore diameter (32, 33). Fragmentation could occur either by disruption of the initial vesicles into smaller membrane fragments, which subsequently reseal into vesicles, or alternatively, by the pinching-off of smaller vesicles in a process analogous to vesicle budding in cellular endo- or exocytosis. The first model would lead to considerable dilution of the vesicle contents, as the vesicle contents exchange with the external medium, whereas the second model would not. To distinguish between these models, we prepared 100-nm myristoleate vesicles encapsulating 20 mM calcein dye, grew the vesicles to 140 nm through slow micelle addition (thus doubling the surface area and increasing the volume by $2\sqrt{2}$) (19). We then extruded the vesicles through 100-nm pores to a final mean size of 88 nm. Separation of vesicles from unencapsulated calcein by size-exclusion chromatography revealed that $\sim 55\%$

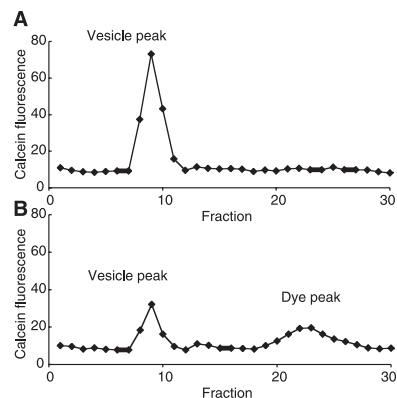


Fig. 5. Vesicle division by extrusion. Panels show size-exclusion chromatography column profiles of 40 mM myristoleate vesicles with 20 mM encapsulated calcein grown to double their surface area at a constant concentration for 4 hours [(A) 100% of dye encapsulated in vesicles] and subsequently divided 24 hours after the beginning of growth [(B) 43% of dye encapsulated in vesicles].

of the dye had been lost from the vesicles during extrusion (Fig. 5, A and B). This is only moderately more dye loss than expected from the volume reduction (38%) resulting from the transformation of 140-nm spherical vesicles into 88-nm vesicles with conservation of surface area. These results indicate that myristoleate vesicles can be forced to divide by the process of extrusion, with only a slightly greater loss of internal contents than that demanded by the geometric constraints of deriving two daughter spheres from one larger parent.

Having shown that both vesicle growth and vesicle division could occur, we carried out repeated cycles of growth and division (19). A population of extruded vesicles was grown by slow feeding with one molar equivalent of myristoleate micelles, and then divided by extrusion. A constant concentration of 40 mM myristoleate was maintained during each step, and the same volume was used at the beginning of each growth cycle. An increase in the intensity of 90° light scattering after each growth phase showed that the average size of the myristoleate aggregates increased, as expected (Fig. 6A). A more detailed quantitative analysis of the average vesicle size by DLS over five cycles of growth and division shows the expected size increase after each 4-hour growth period (Fig. 6B); averaged over all five cycles, the initial

diameter was 88 ± 8 nm, and the diameter after growth was 130 ± 8 nm. The vesicle diameter increased by 1.47 ± 0.17 , close to the expected size increase that would result from 100% incorporation of the added myristoleate (factor of 1.41). Control vesicles stirred under argon but with no micelles added showed insignificant growth by DLS. The amount of encapsulated calcein remaining inside the vesicles was determined by size-exclusion chromatography after each growth period and each division. As expected, essentially no dye was lost during any of the five growth phases (average fraction of dye retained was 1.16 ± 0.19). In contrast, ~40% of the dye was lost after each division (average fraction of dye retained 0.57 ± 0.10). This amount of contents loss is only slightly more than that expected from the decrease in average vesicle size during division (Fig. 6C). Furthermore, we observed a consistent trend toward decreased self-quenching of the encapsulated calcein as it became progressively more dilute during each growth phase, consistent with the expected increase in vesicle volume after the increase in surface area resulting from membrane growth (fig. S4).

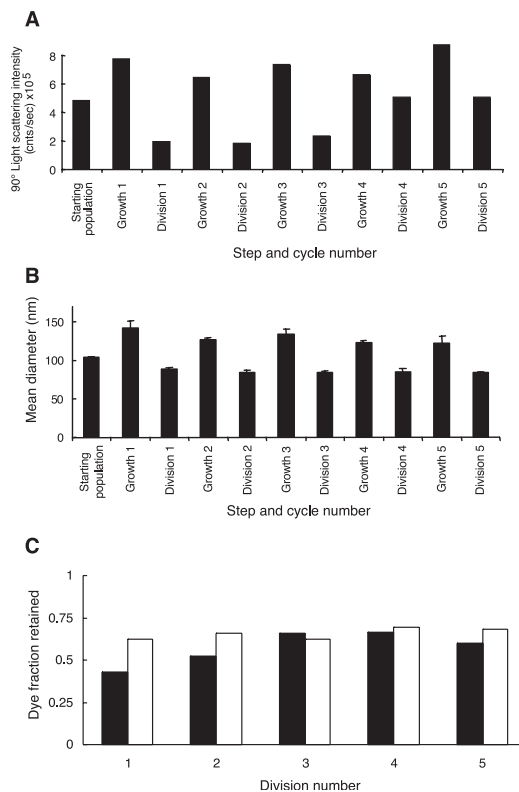
These experiments constitute a proof-of-principle demonstration that vesicle growth and division can result from simple physico-chemical forces, without any complex biochemical machinery. In this system, growth is driven by

the energy associated with a pH-dependent phase change in the lipid from micelles to bilayer membrane. Division, in contrast, is driven by work used to pass vesicle suspensions under pressure through small-pore filters. Although vesicle growth by processes similar to that demonstrated here might occur in a natural prebiotic setting, our use of membrane extrusion to mediate division is artificial, and the possibility of a natural analog of this process seems remote. (Flow through porous rock should be evaluated, however.) An intrinsic membrane curvature resulting from membrane asymmetry might favor spontaneous division by stabilizing the requisite budded-vesicle shape (34, 35).

References and Notes

1. J. M. Gebicki, M. Hicks, *Nature* **243**, 232 (1973).
2. J. M. Gebicki, M. Hicks, *Chem. Phys. Lipids* **16**, 142 (1976).
3. W. R. Hargreaves, D. W. Deamer, *Biochemistry* **17**, 3759 (1978).
4. C. L. Apel, D. W. Deamer, M. N. Mautner, *Biochim. Biophys. Acta* **1559**, 1 (2002).
5. P.-A. Monnard, C. L. Apel, A. Kanavarioti, D. W. Deamer, *Astrobiology* **2**, 139 (2002).
6. D. W. Deamer, *Nature* **317**, 792 (1985).
7. D. W. Deamer, R. M. Pasley, *Orig. Life Evol. Biosphere* **19**, 21 (1989).
8. J. P. Dworkin, D. W. Deamer, S. A. Sandford, L. J. Allamandola, *Proc. Natl. Acad. Sci. U.S.A.* **98**, 815 (2001).
9. T. M. McCollom, G. Ritter, B. R. T. Simoneit, *Orig. Life Evol. Biosphere* **29**, 153 (1999).
10. A. I. Rushdi, B. R. T. Simoneit, *Orig. Life Evol. Biosphere* **31**, 103 (2001).
11. T. H. Haines, *Proc. Natl. Acad. Sci. U.S.A.* **80**, 160 (1983).
12. R. Smith, C. Tanford, *Proc. Natl. Acad. Sci. U.S.A.* **70**, 289 (1973).
13. J. W. Szostak, D. P. Bartel, P. L. Luisi, *Nature* **409**, 387 (2001).
14. J. P. Ferris, G. Ertem, *Science* **257**, 1387 (1992).
15. J. P. Ferris, G. Ertem, *J. Am. Chem. Soc.* **115**, 12270 (1993).
16. G. Ertem, J. P. Ferris, *J. Am. Chem. Soc.* **119**, 7197 (1997).
17. M. Franchi, J. P. Ferris, E. Gallori, *Orig. Life Evol. Biosphere* **33**, 1 (2003).
18. The spontaneous self-assembly of vesicles can readily be observed by the addition of an alkaline solution of fatty acid micelles to a buffered solution at pH 8.5; during the course of the reaction, the turbidity of the solution increases as small 2- to 3-nm micelles (which scatter light very inefficiently) aggregate into patches of membrane and eventually into even larger vesicles of up to many microns (which scatter light much more effectively). This reaction has a long lag phase, but the reaction rate gradually increases due to the autocatalytic effect of preformed vesicles on the formation of new vesicles (36).
19. Materials and methods are available as supporting material on Science Online.
20. L. Ramos, T. C. Lubensky, N. Dan, P. Nelson, D. A. Weitz, *Science* **286**, 2325 (1999).
21. H. Aranda-Espinoza et al., *Science* **285**, 394 (1999).
22. W. K. Johnston, P. J. Unrau, M. S. Lawrence, M. E. Glasner, D. P. Bartel, *Science* **292**, 1319 (2001).
23. P. Walde, R. Wick, M. Fresta, A. Mangone, P. L. Luisi, *J. Am. Chem. Soc.* **116**, 11649 (1994).
24. N. Berclaz, M. Muller, P. Walde, P. L. Luisi, *J. Phys. Chem. B* **105**, 1056 (2001).
25. M. J. Hope, M. B. Bally, G. Webb, P. R. Cullis, *Biochim. Biophys. Acta* **812**, 55 (1985).
26. B. A. Korgel, J. H. van Zanten, H. G. Monbouquette, *Biophys. J.* **74**, 3264 (1998).
27. D. K. Struck, D. Hoekstra, R. E. Pagano, *Biochemistry* **20**, 4093 (1981).

Fig. 6. Multiple cycles of growth and division. (A) 90° light-scattering intensities in counts per second, (B) DLS mean diameters (mean and standard deviation of four measurements), and (C) observed (solid bars) and expected (open bars) dye loss for divided populations during each of five cycles (expected values based on DLS diameters before and after division).



REPORTS

28. V. S. Malinin, M. E. Haque, B. R. Lentz, *Biochemistry* **40**, 8292 (2001).
29. L. D. Mayer, M. J. Hope, P. R. Cullis, *Biochim. Biophys. Acta* **858**, 61 (1986).
30. R. Nayer, M. J. Hope, P. R. Cullis, *Biochim. Biophys. Acta* **986**, 200 (1989).
31. S. G. Clerc, T. E. Thompson, *Biophys. J.* **67**, 475 (1994).
32. D. G. Hunter, B. J. Frisken, *Biophys. J.* **74**, 2996 (1998).
33. B. J. Frisken, C. Asman, P. J. Patty, *Langmuir* **16**, 928 (2000).
34. B. L.-S. Mui, H.-G. Döbereiner, T. D. Madden, P. R. Cullis, *Biophys. J.* **69**, 930 (1995).
35. M. Traïkia, D. E. Warschawski, O. Lambert, J.-L. Rigaud, P. F. Devaux, *Biophys. J.* **83**, 1443 (2002).
36. E. Blöchliger, M. Blocher, P. Walde, P. L. Luisi, *J. Phys. Chem. B* **102**, 10383 (1998).
37. We thank A. Keefe, P. L. Luisi, B. Seelig, P.-A. Monnard, I. Chen, K. Ashtiani-Salehi, and A. Luptak for their helpful comments on the manuscript and P. L. Luisi for helpful discussions and communication of results before publication. This work was supported by grants from the Human Frontier Science Program and the NASA Astrobiology Institute. M.M.H. was supported by an NIH National Research Service Award.

S.M.F. was supported by a National Science Foundation Graduate Research Fellowship. J.W.S. is an Investigator of the Howard Hughes Medical Institute.

Supporting Online Material

www.sciencemag.org/cgi/content/full/302/5645/618/DC1

Materials and Methods

Figs. S1 to S4

References

31 July 2003; accepted 24 September 2003

Glacial Earthquakes

Göran Ekström,^{1*} Meredith Nettles,¹ Geoffrey A. Abers²

We have detected dozens of previously unknown, moderate earthquakes beneath large glaciers. The seismic radiation from these earthquakes is depleted at high frequencies, explaining their nondetection by traditional methods. Inverse modeling of the long-period seismic waveforms from the best-recorded earthquake, in southern Alaska, shows that the seismic source is well represented by stick-slip, downhill sliding of a glacial ice mass. The duration of sliding in the Alaska earthquake is 30 to 60 seconds, about 15 to 30 times longer than for a regular tectonic earthquake of similar magnitude.

Most earthquakes follow a simple scaling relationship such that the duration of fault movement is proportional to $10^{M/2}$, where M is the earthquake moment magnitude. The typical duration of an $M = 5$ earthquake is 2 s, and an $M = 7$ earthquake, 20 s. The short duration of seismic energy release leads to efficient radiation of high-frequency ($f \sim 1$ Hz) seismic waves, and first-arriving, high-frequency P waves are traditionally used to detect and locate seismic events. Earthquakes with durations much longer than normal radiate less energy at the frequencies used for earthquake monitoring and may go undetected.

Earthquakes with durations of thousands of seconds cannot be detected by seismometers because they do not generate elastic waves. Such earthquakes have, however, been detected geodetically (1–5). Very-long-period (1 to 10 mHz) seismic data have been used in attempts to detect and locate moderate and large ($M \geq 5.0$) earthquakes with durations of tens to hundreds of seconds, with ambiguous results (6–8).

Here, we use a recently developed method (9) to detect and locate sources of long-period seismic surface waves on a global scale. The detection and location algorithm has its basis in standard array-processing techniques. Vertical-component seismograms from about 100 seismometers around the world are filtered between 35- and 150-s period and phase adjusted to correct for Rayleigh wave propagation delays from a given test location to each station. Any

Rayleigh wave signal emanating from the test location will then be in phase across the stations of the global array, and the signals

can be analyzed for the simultaneous presence of coherent energy (fig. S1). Continuous seismic data are analyzed for detections on a dense grid of test locations covering the surface of the Earth (10).

Application of the algorithm to 3 years of data, 1999 to 2001, has led to the detection and location of 7292 events. The smallest earthquake detected has an estimated magnitude (M) of $M = 4.6$. All but 521 of the events are correlated spatially and temporally with earthquakes already reported in various global bulletins of seismicity. Of the 521 previously unknown events, about 450 occur along plate boundaries or in other tectonically active zones. Many are located along the ridge-transform system in the Southern

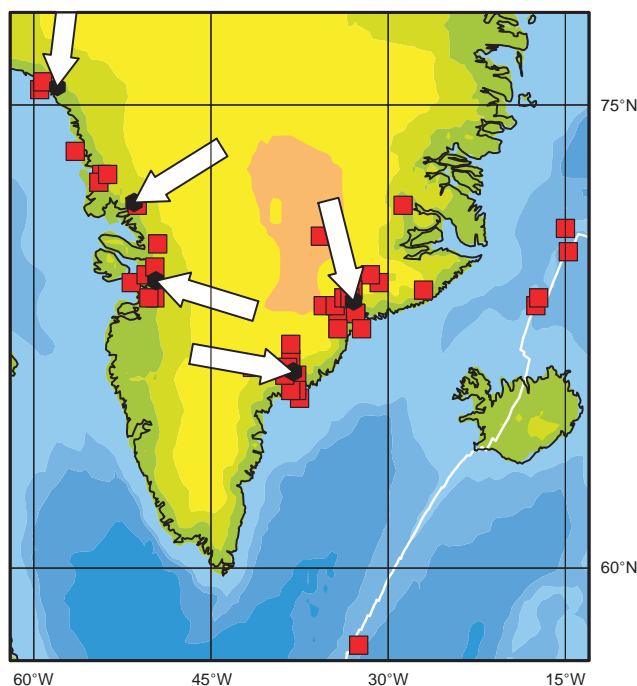


Fig. 1. Topographic map of southern Greenland and vicinity. The white line shows the location of the northern mid-Atlantic ridge. Red squares show the locations of detected earthquakes not previously reported in the earthquake bulletins of the NEIC or the ISC. Five previously unknown earthquakes were detected in the seismically active region near the plate boundary, and 42 previously unknown earthquakes ($4.6 \leq M \leq 5.0$) were detected near the coast of Greenland. White arrows show the horizontal slip azimuths obtained in CSF inversions of teleseismic data for five well-recorded events (on 19 April 1999, 24 April 1999, 16 August 2000, 15 September 2000, and 28 December 2001; see table S1). The black hexagon at the tip of each arrow indicates the centroid location obtained in the inversion.

¹Department of Earth and Planetary Sciences, Harvard University, 20 Oxford Street, Cambridge, MA 02138, USA. ²Department of Earth Sciences, Boston University, 685 Commonwealth Avenue, Boston, MA 02215, USA.

*To whom correspondence should be addressed. E-mail: ekstrom@seismology.harvard.edu